FEM ANALYSIS OF INTERNAL STRESS SUPERPLASTICITY IN AL/SIC$_W$ COMPOSITE WITH DIFFERENT V_F SUBJECTED TO THERMAL CYCLING

Ali Abedian, Ali Malekpour
DEPARTMENT of AEROSPACE ENGINEERING,
SHARIF UNIVERSITY of TECHNOLOGY,
Tehran, Iran

Keywords: *Superplasticity, Metal Matrix Composite (MMC), FEM, and Axisymmetric Model*

Abstract

Special specifications of whiskers reinforced Metal Matrix Composites (MMCs) have made these materials very attractive for the aerospace applications. However, it is so difficult to conform these materials to complex shapes. In recent years, some experimental attempts have been made to extend the borders of superplasticity science to promote superplastic characteristic of MMCs. But, a few numerical studies would be found on the simulation of the superplastic process. In the present study it is tried to highlight the difficulties involved with the FEM modeling of superplasticity in MMCs. The results of this simulation work are very promising and have shown a reasonable agreement with the experimental results available on the Internal Stress Superplasticity (ISS) tests and strain-rate-sensitivity data. Specifically, the strain rate vs. stress diagrams obtained from the simulation and experiments show an acceptable correlation.

1 Introduction

The low density and high modulus of whiskers reinforced Metal Matrix Composites (MMC) have made these materials very attractive for the aerospace applications. But, it is so difficult to conform these materials to complex shapes, due to the following reasons. First of all, they exhibit very poor ductility and formability at both room and elevated temperatures due to the large volume fraction of the ceramic reinforcements. Secondly, they are often quite difficult to machine [1]. In recent years, the borders of superplastic experience with the conventional materials have been extended to the area of composite materials. Many experiments have been designed to explore and clarify the best mechanisms of superplastic deformation in these materials [2-5]. The studies have indicated that the loading condition of simultaneous thermal cycling and application of a low mechanical stress is the best way for enforcing MMCs to undertake superplastic deformation [1-3,6-12].

Two different types of regulating mechanisms of superplastic deformation in polycrystalline materials have been observed. The first type is termed as the Fine Structure Superplasticity (FSS) and the other is referred to the Internal Stress Superplasticity (ISS). FSS refers to the phenomenon of extensive elongation in materials with fine-grained structures. The ISS, on the other hand, refers to the phenomenon of extensive elongation in materials having high internal residual stresses. Thermal cycling in any one of the following systems can generate the residual stresses. First, materials having phase transformations through a thermal cycling regime as in iron and in Fe-Ni alloys. Second, materials with anisotropic thermal expansion coefficients as in zinc and α-uranium. Third, materials having phases with different thermal expansion coefficients as in aluminum containing SiC whiskers and zinc

containing Al_2O_3 [8]. Therefore, for the case of Al-SiCw composite, due to the different coefficients of thermal expansions (CTEs) between the SiC whiskers and the aluminum matrix, superplastic deformation under thermal cycling condition can be promoted in the material.

Some analytical models have been introduced for simulation of superplastic deformation in composites [6]. These models are based on two different types of the previously proposed mechanisms for the superplasticity. One mechanism is the development of an idea initially put forward by Roberts and Cotterell [13] in which the internal stress effectively determines the enhanced deformation. In the absence of an applied external stress the local differences in CTE will, given a sufficiently large thermal excursion, generate an internal stress in excess of yield stress and consequently causes plastic flow. On thermal cycling this flow will settle down into a fully reversible regime. If there is an external stress this will bias the internal plastic flow in its direction and results in an increment of plastic strain in the same direction in each cycle. This was developed into a more soundly based quantitative predictive model using the Levy-Von Mises flow rules and has been further developed for other cases of the phenomenon [14,15]. These models produce a mean for prediction of a linear relationship between the extra strain per thermal cycle ($\Delta\varepsilon$) and the external stress (σ_x) such that;

$$\Delta\varepsilon = \frac{5C_1(\Delta V/V)}{3\sigma_y}\sigma_x \qquad (1)$$

where $(\Delta V/V)$ represents the fractional constrained change in the volume generated during each thermal cycle, σ_y is the material yield stress, and C_1 is a constant closed to 1. In a power-law formulation, this results in an immediate change in the creep rate ($\dot{\varepsilon}$) to;

$$\dot{\varepsilon} = A(\sigma_x + \sigma_i)^n \qquad (2)$$

where σ_i is the internal stress and A and n are constants of the creep equation. The net strain per cycle will then be the sum of the integral of the strain rates over the thermal cycle;

$$\Delta\varepsilon = \int A(\sigma_x \pm \sigma_i)^n dt \qquad (3)$$

where the sign of σ_i depends on whether the heating or cooling part of the cycle is in progress. If $\sigma_i >> \sigma_x$ and if σ_i does not recover during the cycle, then equations (2) and (3) will reduce to;

$$\dot{\varepsilon}^* = nA(\sigma_i^*)^n\sigma_x \qquad (4)$$

where $\dot{\varepsilon}^*$ is the mean strain rate and σ_i^* is the mean internal stress averaged over the thermal cycle. This approach has been used in conjunction with the plastic rule model to simulate the phenomenon where there is insufficient internal strain to generate plastic flow and also in place of the plastic flow rule model in a more developed form [16]. In these models σ_i^* is taken very close to σ_y if matrix yield occurs during cycling. To understand the deformation mechanisms and the inter-relationship between the constituents of the composites in the event of superplastic behavior, it is necessary to analyze the problem carefully.

As the experimental works are time consuming, costly, and are very equipment dependent, analytical and numerical studies, which have not widely been considered, must be developed. However, since the analytical studies involve very complicated PDEs and require so many assumptions to become solvable, numerical methods such as the Finite Element Method (FEM) may ease the solution, though very careful geometry and material modeling, as well as the meshing, and employing nonlinear procedures (such as stepping and updating the stiffness matrix in each step) are necessary. It should be mentioned that due to the complications involved only a few FEM studies would be found in the literature [17]. In the present study it is tried to highlight the

difficulties involved with FEM modeling of superplasticity in MMCs. Also, the effects of fiber volume fraction, plastic behavior of the matrix, and the fiber/matrix debonding on the superplastic behavior of the composites are carefully studied.

2 Geometry, Loading and Material Modeling

For reducing the cost of calculations and overcoming the hardware and software limitations, it is necessary to adopt some simplification assumptions regarding the geometry modeling. The SEM photos of the cross-section of MMCs have shown that the added SiC_w to the aluminum matrix are dispersed in the direction that they are extruded [18]. The photos show that the misalignment of about 30% of the whiskers is limited to $\pm 9.3^{o}$ where the rest are more or less aligned. Therefore, it could be assumed that the fibers are of circular cross-section and aligned as shown in Fig. 1(a). Such an assumption makes it possible to simulate the whole composite with an axisymmetric micromechanical model, see Fig. 1(b). The applied boundary conditions are presented in Fig. 1(c). Since the fiber/matrix debonding is an important factor in controlling the composite deformation, as it has been the case for creep behavior of MMCs [19], this phenomenon is considered in this study, as well. Fig. 2 shows different situation of debonding at fiber/matrix interface. However, it should be noted that the fiber misalignment, fiber offsetting, and the fiber and unit cell geometric ratios (aspect ratios), which could also affect the rate of deformations are ignored here. As for the meshing, uniform quadrilateral elements were considered. But, it should be noted that an extra ordinary stress filed is developed at the sharp corner of the fiber, where for computing the effects of this field on the inelastic behavior of the material, it is necessary to place very fine mesh in this region [19].

This effect has been added to the study and the results will be published in a separate paper. The fiber volume fraction (V_f) is calculated as shown by equation (5);

$$V_f = (\frac{r}{b})^3 \frac{AR_f}{AR_u} \qquad (5)$$

where r and b are the fiber and the unit cell radii, and AR_f and AR_u are the fiber and the unit cell aspect ratios, respectively. Here, volume fractions of 10 and 20 percent and AR_f=4 are considered [8]. Plane-82 of ANSYS element library, which is a 2-D axisymmetric nonlinear elasto-visco-plastic element, was used for the geometry meshing.

In this study it is assumed that the fibers remain elastic during the whole process, while the 2024Al matrix behaves in an elastic perfectly plastic manner and for 6061Al matrix both elastic-perfectly plastic and elaso-visco-plastic behavior are considered. The properties assumed for the fiber and matrix are presented in Table 1.

Table 1- Materials properties for Al – SiCw

MATERIAL	E (GPa)	CTE (K^{-1})	ν	σ_y (Mpa)
2024 Al	73	24.7 x 10^{-6}	.33	30
6061 Al	69	23.6 x 10^{-6}	.345	30
SiC	470	4.6 x 10^{-6}	.17	-

Also, creep behavior of 6061Al is modeled with Nieh equation as follow [20];

$$\dot{\varepsilon} = 2x10^{13}\sigma^{4.0} \qquad (6)$$

As for the loading, according to the literature available on the experimental superplasticity, it is assumed that a thermal cycling regime as in Fig. 3 along with a small constant mechanical stress are applied to the model. For the heating phase of the cycle, the composite is heated between 100°C-450°C in only 50 seconds, while it is cooled down to 100°C from the maximum of 450°C during 150 seconds [8]. This thermal cycle is accompanied with a constant longitudinal small mechanical stress of magnitude 2, 4, 7, and 10MPa [8] to

form the biased stress for promoting superplastic deformation.

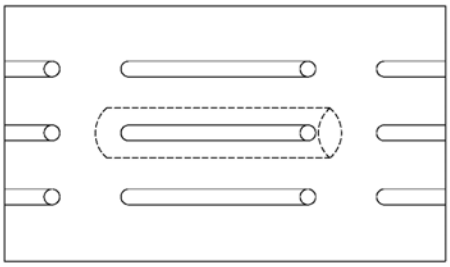

(a)

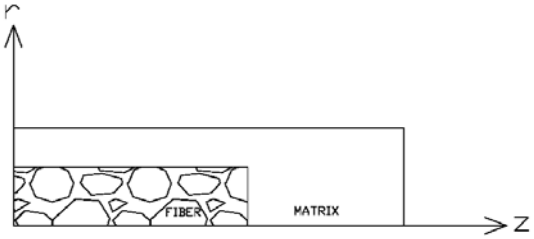

(b)

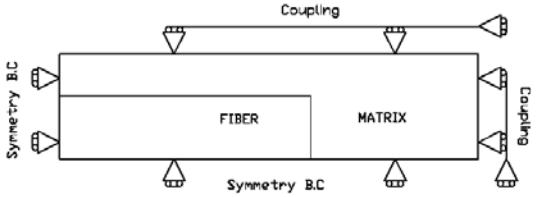

(c)

Fig. 1 Geometry modeling of fiber and matrix, (a) fiber and matrix situation in 3-D modeling, (b) fiber and matrix situation in 2-D modeling, (c) the final modeling of fiber and matrix with symmetric boundary condition

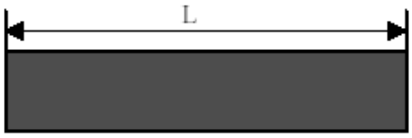

(a)

(b)

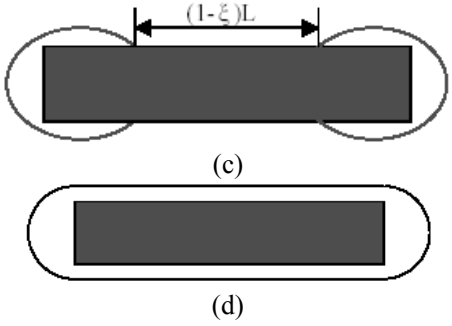

(c)

(d)

Fig. 2 Different situation of debonding at fiber/matrix interface, (a) perfect bonding, (b) fiber end bonding, (c) partial debonding, (d) full debonding

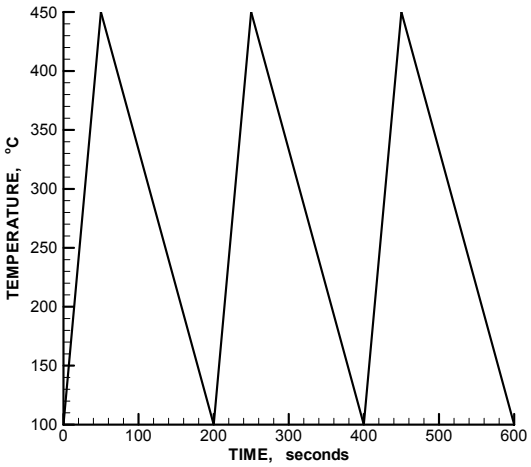

Fig. 3 Thermal cycle loading

3 Results and discussion

As it was explained before, the residual internal stresses in composites can be directed in a way that promotes superplastic deformation in these materials. Applying a very high amplitude thermal cycle can generate a very high thermal stress in the matrix, which will have a tensile nature in the cooling phase and a compressive nature in the heating phase of the cycle, provided that the CTE of the matrix is large enough compared to that of the fiber. If the magnitude of the cyclic thermal stress is higher than the σ_y of the matrix (considering a unidirectional effect), the tensile and

compressive plastic strains generated in each phase of the cycle will relatively vanish. In order to create a controlled plastic deformation in these materials (i.e. avoid necking), a small constant stress is recommended to be accompanied by the thermal cycle to bias the generated thermal stress during the cyclic heating. As a result, the plastic deformation starts to accumulate with increasing the number of cycles. Considering a perfect bound at the fiber/matrix interface, no initial residual stress and strain for the composite, elastic fiber, elastic-perfectly plastic behavior for the matrix, and the most importantly assuming that the matrix has no intrinsic strain-rate-sensitivity (i.e. m=0), the graph of accumulated plastic strain with the number of cycles could help to understand the deformation mechanisms happen in the material under the loading condition.

The above mentioned graph (ε vs. N) for 2024Al / 20%SiC$_w$ composite assuming perfect a bound between the fiber and matrix and under four different applied stress of 2, 4, 7, and 10 MPa is shown in Fig. 4. Note that the matrix behavior was considered to be elastic-perfectly plastic. Since the plastic strain for all four cases is linearly increased with N, the strain rate for the thermal cycling could be calculated using equation (7);

$$\dot{\varepsilon} = \frac{d\varepsilon}{dN}.\frac{1}{\tau} \qquad (7)$$

where $d\varepsilon$ is the accumulated strain in the given number of cycles (i.e. dN) and τ is the period of the cycle [8].

Using the calculated $\dot{\varepsilon}$ for each case, the stress exponent under the applied stresses could be found by plotting $\dot{\varepsilon}$ vs. σ in log-log scale. Fig. 5 shows the results estimated by the FEM simulation.

As it is seen from the graph in the log-log scale, a linear relationship between σ and $\dot{\varepsilon}$ could be estimated. This means that a relationship of power law type (i.e. $\dot{\varepsilon} = A\sigma^n$) could be considered between the strain rate and applied stress. Note that the order n=1 is defined as the condition of Newtonian viscous flow, which is required to promote superplastic deformation in composites. For the verification of the performed FEM modeling, the experimentally measured results for the same composite under similar loading and test conditions are presented in Fig. 5. As the figure shows, the fitted lines to the experimental and FEM data are relatively parallel. From the graphs, the value of n for the experimental and FEM results appears to be 1.6 and 1.8, respectively. These values of n indicate a kind of Newtonian viscous flow. It is reminded that under isothermal loading condition the composite behavior would substantially different where the exponent n appears to be a number close to 8 [8]. Note also that though the order n obtained from the FEM and experimental works are similar, but the difference between the $\dot{\varepsilon}$ values for the applied stresses is of importance as it is seen, for lower stress levels the difference between the calculations and the measurements are higher. This may be due to the much small plastic strain values, which need very precise tools to correct data. Moreover, this could happen due to the simplifications considered for FEM modeling of both the geometry and materials and also the way of simulation of the loading and test conditions, which are currently under investigation. For better understanding of the plastic deformation of the composite under the applied loading regime, a graph of cyclic plastic strain for 40 loading cycles under the stress levels of 7 and 10MPa are shown in Fig. 6. As the figure shows, the cumulative residual plastic strain appears to increase linearly with time. The bias effect of the applied constant stress causes a small difference between the tensile and compressive plastic strains in the cooling and heating phases of the thermal cycle, which the differences accumulate during the successive loading cycles. These graphs also reconfirm the linear relationship between the plastic strain and the number of cycles (N).

To get a clear picture of the plastic strain distribution through out the model, this quantity for cycle=40 and σ=7MPa is shown in Fig. 7. As it is seen, the sharp corner region of the fiber is the focal point for the plastic strain field. The excessive element distortion in this corner

causes slow convergence of the results and to get fast and acceptable solution it is required to treat this area very carefully. It is noted that any change in the fiber geometry in this corner may effect the results to a great extend which is currently under investigation. As Fig. 7 shows the deformation after 40 cycles in the composite is enormous.

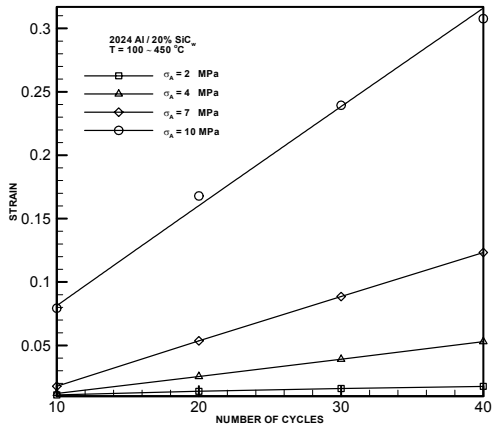

Fig 4 ε vs. N graph for 2024Al/20% SiC_w

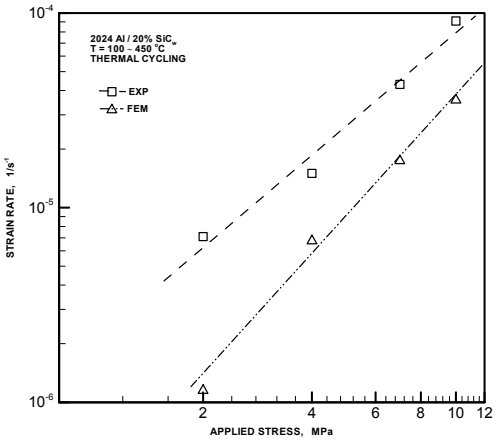

Fig. 5 Comparison between FEM and experimental data for 2024Al/20%SiC_w

Repeating the analysis for a similar composite with V_f =10% shows again that the graphs of strain vs. the number of cycles (N) for all four cases of σ=2, 4, 7, and 10MPa are linear. Therefore, calculating the strain rate from Eq. 6 will be possible. Fig. 8 presents a comparison between the FEM calculation and the experimental measurements [8] of $\dot{\varepsilon}$ vs. σ in log-log scale. Though the calculated values of $\dot{\varepsilon}$ for all the applied stress cases are different with that of the measurements, but the exponent n for the FEM modeling is found to be 1.9 where it is 1.8 for the experimental results. The correlation of the results is very interesting. It is reminded again that based in the literature for n<3 (or m=1/n>0.33, strain rate sensitivity exponent) the composite shows superplastic deformation and right at n=1 a perfect Newtonian viscous flow occurs. Interestingly, the calculated strain rate sensitivity exponents m=0.53 while its 0.56 from the experiment.

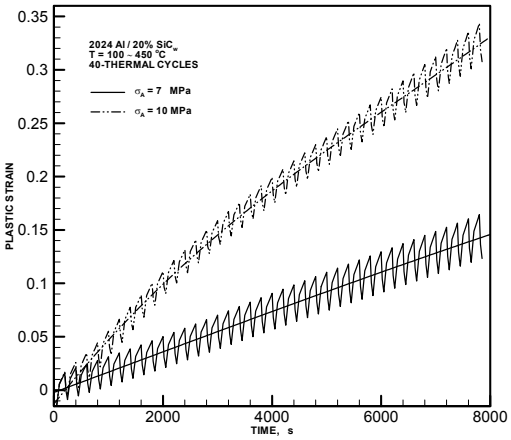

Fig. 6 Plastic strain vs. time graph for 7 and 10MPa applied stresses in 2024Al/20%SiC_w

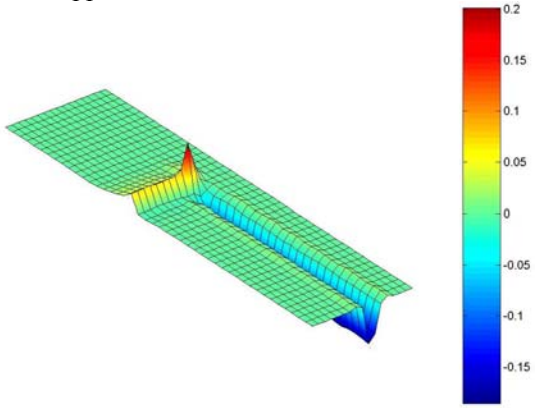

Fig 7. Plastic strain distribution for 7MPa applied stress after 40 thermal cycles in 2024Al/20%SiC_w

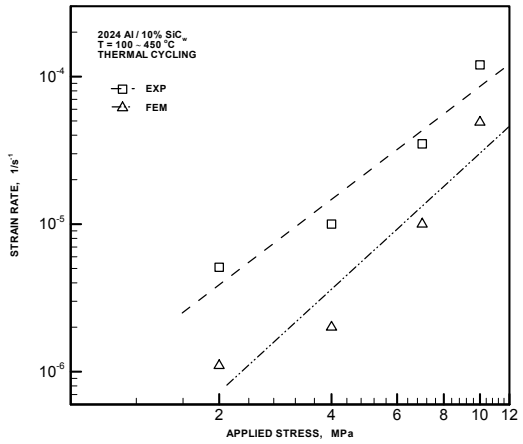

Fig. 8 Comparison between FEM and experimental data for 2024Al/10%SiC$_w$

A comparison of the results obtained from V_f =10% and V_f =20% shows interesting findings. With decreasing the fiber volume fraction from 20% to 10% the order of n increases from 1.8 to 1.9, which is exactly similar to what happens with the measured n from the experiments, see Fig. 9 and 10.

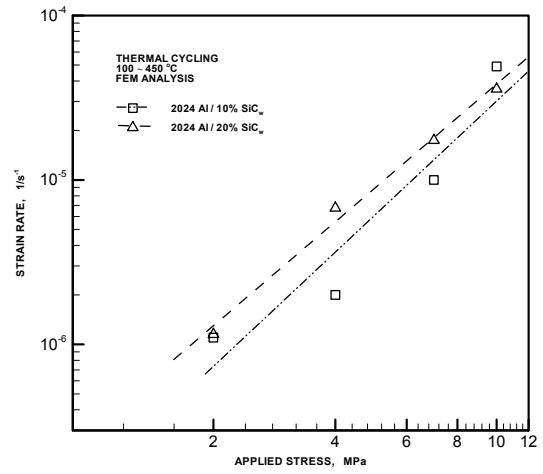

Fig. 9 Comparison of FEM data between 2024Al/20%SiC$_w$ and 2024Al/10%SiC$_w$

It could be explained with this fact that higher V_f results in higher surfaces of contact between the fiber and matrix, which this in turn increases the level of internal residual thermal stresses in the composite. Therefore, with this, it is expected that the composite get closer to the regime of Visco-Newtonian flow. It is reminded again that for n<3 or m=1/n>.33 (strain rate sensitivity) the material shows more aspect of the Newtonian viscous flow, where n=1 is the condition of perfect Newtonian viscous flow. With decreasing V_f , the plastic flow in the composite decreases, where at a critical level of V_f , the ISS supperplastic regime would not be effective any more. This has been experimentally shown that V_f <0.5% is the critical point [17] and in this situation the FSS regime, which is based on the grain structure of the matrix and the distribution of the fibers in the matrix, will be the controlling regime of the superplastic behavior of the composite. Looking at Fig. 9 and 10 shows another important thing that should be noted. At lower applied stresses the calculated strain rate is smaller for V_f =10% compared to the values for V_f =20%. However, at σ=10MPa, this is reversed at the strain rate for V_f =10% becomes higher than that of the V_f =20%. This is exactly similar to what happens for the experimental measurements of $\dot{\varepsilon}$ for V_f =10% and 20%, see Fig. 10. This is still numerically under investigation.

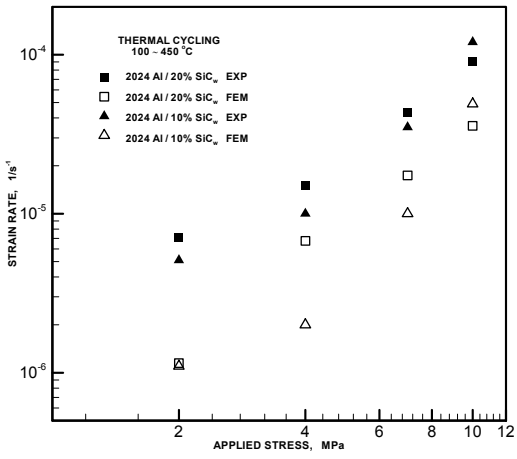

Fig. 10 Comparison between FEM and experimental data for 2024Al/SiC$_w$ with 10% and 20% V_f

However, as Fig. 10 shows, though the calculated and the measured n are close, but the difference between the corresponding $\dot{\varepsilon}$ (i.e. FEM and the experimental tests) is still high.

This could be attributed to the ignorance of the following physical aspects of the composite by the FEM study, i.e. fiber misalignment, fibers overlapping, fiber/matrix debonding, different fiber dimensions, effect of the supperplastic deformation of the composite on the changes to the degree of the homogeneity of the composite [8], matrix strain rate sensitivity, matrix strain hardening, matrix elasto-visco-plastic behavior, etc. Of course, the details of the loading conditions for the FEM and the experimental studies are different, which should be taken into account.

To check upon the above parameters, here the fiber/matrix debonding, which has been found to be an important factor for the prediction creep behavior of MMCs [18-20], is incorporated into the FEM modeling. Based on the available literature, the debonding parameters ξ is changing from zero to 1, where ξ=1 will mean full debonding and ξ=0 corresponds to fiber end debonding, see Fig. 2. Here, the modified model with ξ=0.25 is considered. The same loading conditions as were applied to the model without debonding are applied in here.

As Fig. 11 shows, under the applied mechanical loads of 2, 4, 7, and 10MPa, the relationship between the strain and the number of cycles is linear, therefore the strain rate could be measured from Eq. 7. The changes in strain rate vs. the applied stress for the models with and without debonding are shown in Fig. 12. For comparison, the experimental data are also presented in this figure. As it is clear from the figure, with considering the debonding, the calculated strain rate gets closer to the experimental data. However, the strain rate sensitivity seems to be increases. These changes are still under consideration and to find a reasonable explanation it is necessary to study the effects of ξ on the results.

In this study, the effect of elasto-visco-plastic behavior of the matrix was also considered. In this regard the 6061Al / 20%SiC_w composite was modeled both the options of elasto-perfectly plastic and elasto-visco-plastic for the matrix. Under the applied thermal cycles and the mechanical stresses (i.e. σ=2, 4, 7, and 10MPa), it was found for the option of elasto-perfectly plastic that the relationship between the plastic strain and the number of cycles is higher and the graph of strain rate vs. the applied stress provides n=1.24, which is closed to the experimental value of n=1[11], see Fig. 13.

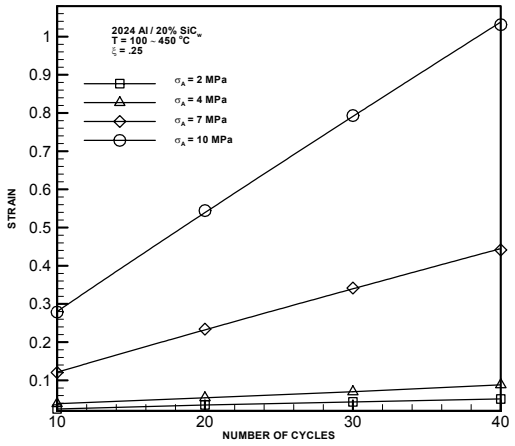

Fig 11 ε vs. N graph for 2024Al/20% SiC_w With ξ=0.25

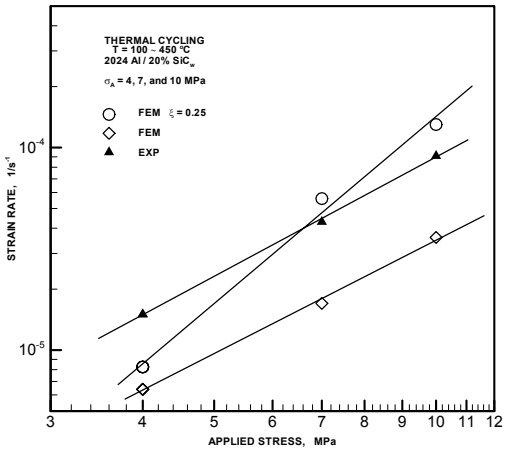

Fig. 12 Comparison of FEM and experimental data for 2024Al/20%SiC_w with and without debonding with applied stresses of 4, 7, and 10MPa

Inclusion of the elasto-visco-plastic behavior of the matrix shows that under the applied thermal cycles and the mechanical

loading regime, the creep response of the matrix is negligible and the superplastic response is the dominating behavior for the composite.

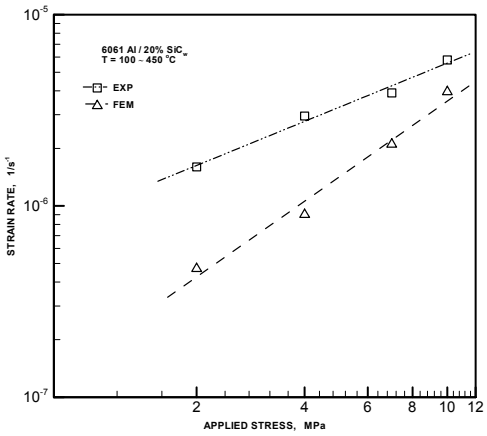

Fig. 13 Comparison between FEM and experimental data for 6061Al/20%SiC$_w$

It is noted that for the composites with a small difference between CTE of the fiber and matrix and also the case with high CTE, which is under a constant temperature, the creep deformation is the dominating phenomena [1,8,11,15].

For compilation of the discussion about the material behavior, the effects of the strain hardening of the matrix on the superplastic behavior of the composites is still under consideration and the results will be published in a separate paper.

4 Conclusions

Considering the results obtained from the FEM modeling of MMC composites, the followings could be calculated:

1) The axisymmetric FEM model could predict the superplastic behavior of the MMC composites to a great exact. Though, it is necessary to include more parameters of the geometry, material properties, and the loading aspects.
2) The strain rate sensitivity obtained from the FEM modeling confirm to the experimental data. However, the calculated and measured strain rates at different applied stresses differ in some extant.
3) Similar to the experimental findings the FEM results show that the strain rate sensitivity value is highly dependant to the fiber volume fraction. With decreasing V_f , the composite behavior distances from the Newtonian viscous flow.
4) The fiber/matrix debonding parameter ξ corrects the calculated strain rates at different applied stresses, however to find the exact effect of ξ on the strain rate sensitivity more modeling studies are necessary.
5) Creep behavior of the matrix under the applied loading conditions does not play an important role in the deformation of the composite. Though, still the strain hardening effect of the matrix must be taken under consideration.

References

[1] Chen Y.C., Daehn G.S and Wagoner R.H. The Potential for Forming Metal Matrix Composite Component via Thermal Cycling. Scripta Metal. Mater., vol. 24, pp. 2157-2162, 1990.

[2] Pickard S.M. and Derby B. The Deformation of Particle Reinforced Metal Matrix composites During Temperature Cycling. Acta Metal. Mater., vol. 38, No. 12, pp. 2537-2552, 1990.

[3] Sunder R.S., Kitazono K., Sato E. and Kuribayashi K. Internal Stress Superplasticity in an In-situ Intermetallic Matrix Composite. Materials Science Forum, Orlando, USA, vols. 357-359, pp. 405-410, 2001.

[4] Sosa S.S. and Langdon T.G. Deformation Characteristics of a 3Y-TZP/20%Al2O3 composite in Tensile Creep. Material Science Forum, vols. 357-359, pp. 135-140, 2001.

[5] Han J. S., Kim M. S., Joeng H. G., and Yamagata H. High Strain Rate Superplasticity in Al-16Si-5Fe Based Alloys with and without Sic Particles. Material Science Forum, vols. 357-359, pp. 613-618, 2001.

[6] Pickard S. M and Derby B. Superplasticity During Thermal Cycling. Fundamental Relationship Between Microstructure and Mechanical Properties of MMC, Indianapolis, pp. 103-113, 1990.

[7] Wu M Y. and Sherby O.D. Superplasticity in a Silicon Carbide Whisker Reinforced Aluminum Alloy. Scripta Metallurgica, vol. 18, pp. 773-776, 1984.

[8] Hong S. H., Sherby O.D., Divecha A. P., Karmarker S. D. and MacDonald B. A. Internal Stress Superplasticity in 2024 Al-SiC Whisker Reinforced Composites, Journal of Composite Materials, vol. 22, pp. 102-123, 1988.

[9] Le Flour j. c. and Locicero R. Influence of Internal Stresses Induced by Thermal Cycling on the Plastic Deformation Resistance of an Al/SiC Composite Material. Scripta Metall., vol. 21, pp. 1071-1076, 1987.

[10] Schuh C. and Dunand D.C. Transformation Superplasticity of Ti-6Al-4V and Ti-6Al-4V/TiC Composites at High Stresses. Materials Science Forum, Orlando, USA, vols. 357-359, pp. 177-182, 2001.

[11] Gonzalez-Doncel G., Karmarker S. D., Divacha A. P. and Sherby O. D. Influence of Anisotripic distribution of Whiskers on the Asuperplastic Behavior of Al in a Back-Extruded 6061Al-20%SiCw Composite. Composites Science and Tech., vol. 35, pp. 105-120, 1989.

[12] Daehn G. S. and Gonzalez-Doncel G. Deformation of Whisker-Reinforced Metal Matrix Composites Under Changing Temperature Conditions. Metal. Trans., vol. 20A, pp. 2355-2368, 1989.

[13] Roberts A.C. and Cottrell A.H. Creep of Alpha Uranium During Irradiation with Neutrons. Phil. Mag., vol. 1, pp. 711, 1956.

[14] Greenwood G.W. and Johnson R.H. The Deformation of Metals under Small Stresses During Phase Transformations. Metal Science J., vol. 6, pp. 33, 1972.

[15] Derby B. Internal Stress Superplasticity in Metal Matrix Composites. Scripta Metall., vol. 19, pp. 703, 1985.

[16] Wu M.Y., Wadsworth J. and Sherby O.D. Internal Stress Superplasticity in Anisotropy Polycrystalline Zinc and Uranium, Metall. Trans., vol. 18A, pp. 451, 1987.

[17] Zhang H., Daehn G. S. and Wagoner R. H. Simulation of Plastic Response of Whisker Reinforced Metal Matrix Composites under Thermal Cycling Conditions. Scripta. Metal. Mater., vol. 25, pp. 2285-2290, 1991.

[18] Lilholt H. and Taya, M. Creep of SiC whiskers/2124 Aluminum Composite. in ICCM-VI/ECCM-II, Matthews.F.L, Buskell, N.C., Hodgkinson, J.M., and Morton, J., ed., vol.2, pp.234-244,1987.

[19] Abedian A. and Mondali, M. FEM study of constant rate creep Analysis of MMCs, 11th Iranian Annual Conference (International) of Mechanical Engineering, vol.3, pp.1271-1280, 2003.

[20] Nieh T.G. Creep Rupture of Silicon Carbide Reinforced Aluminium Composite, Metall. Trans, vol. 15A, pp.139, 1984.